Body-Resonance Human Body Communication

Samyadip Sarkar[1], Qi Huang[1], Sarthak Antal[1], Mayukh Nath[1] and Shreyas Sen[1*]

[1*]School of Electrical and Computer Engineering, Purdue University, West Lafayette, 47907, Indiana, USA.

*Corresponding author(s). E-mail(s): shreyas@purdue.edu;
Contributing authors: sarkar46@purdue.edu;
huan2065@purdue.edu; santal@purdue.edu;
nathm@alumni.purdue.edu;

Contents:

Supplementary Material

Supplementary Discussion 1: Current Density and H-field Distribution:

We present a comparative analysis of the current density and magnetic field distribution via numerical electromagnetic analysis between the EQS and BR frequency regimes, illustrated in Fig. 1.

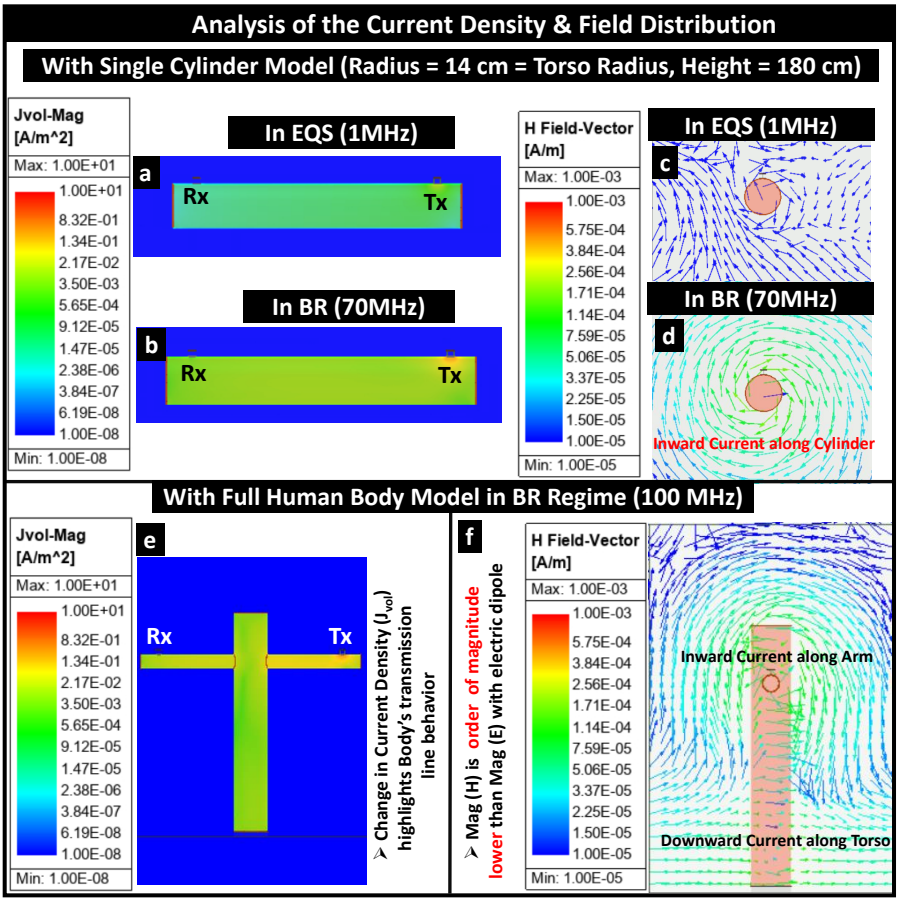

Fig. 1 Supplementary Figure 1: Analysis of Current and H-Field Distribution: with Single Cylinder Model: The complex magnitude of the current density (Jvol) over the volume: **a.** In EQS, **b.** In Body-Resonance, Comparison of the magnetic field vector: **c.** In EQS, **d.** In BR, **with Cross-Cylindrical Human Body Model in BR at 100 MHz: e.** Current Density variation over the volume of the body, **f.** H-field vector

When the operating wavelength (λ) greatly exceeds the maximum dimension of on-body channels (i.e., $\lambda >> l_{Body}$) in the EQS regime, a consistent potential exists throughout the cylindrical body model, resulting in a uniform

current distribution. Conversely, in the BR regime, where the wavelength λ is comparable to the body channel length, there is an increased non-uniform current distribution within the conductor. This variability in current density inside the volume of the human body affirms its conceptual model as a lossy transmission, delineated in Fig. 1 (b, e).

Furthermore, the direction of the H-field indicates the direction of the current carried by the human body. In the EQS regime, the induced H-field is significantly lower than the induced E-field with an electric dipole, allowing us to disregard the influence of the H-field, shown in Fig. 1 (c). Nonetheless, the shift in the direction of the H-field vector, as shown in Fig. 1 (d, f), confirms the unbalanced, lossy transmission line nature of the human body, with the body as a signal conductor and the earth's ground acting as a ground conductor. We have included an animation plot illustrating the variation in H-field with frequency as Supplementary Movie 2 with this manuscript: https://github.com/SparcLab/BodyResonanceHBC

Supplementary Discussion 2: Behavioral Difference of BR HBC in Machine-Machine (M2M) vs Wearable-Wearable (W2W) Scenario

In the context of capacitive HBC, communication devices are known to be classified based on the size of their ground and their coupling to the earth's ground as follows: (a) Machines: These devices have their ground connected to the earth's ground, resulting in higher channel gain that solely depends on the path loss incurred from the body channel. They can also be referred to as ground-connected devices. (b) Wearables: These small form factor, battery-operated devices experience high impedance in their return path (Z_{retTx}, Z_{retRx}) that results from lower return path capacitance ($C_{retTx}, C_{retRx} \sim\leq 1$ pF) [1] due to reduced parasitic ground coupling and can also be referred as ground-floated devices. (c) Tabletop devices: These small devices, when placed on a table, experience unrealistically lower impedance in the return path in comparison to the wearable-to-wearable scenario owing to their return path capacitance lying in the range of 100 -200 pF [2]. For EQS HBC, with voltage mode communication and capacitive termination at the receiver, the change in the setup from Machine-Machine (M2M), Wearable-Wearable (W2W) to Tabletop results in primarily the change in the received signal level (i.e., $V_{Rx-M2M} >> V_{Rx-Tabletop} >> V_{Rx-W2W}$).

However, in BR HBC, the operational frequency range, i.e., the location of the BR peak, changes with the setup as the M2M/M2W setup shifts the peak to a lower frequency than the W2W setup. With the M2M/M2W setup, the human body acts like a quarter wave monopole (i.e., $f_r \propto \frac{1}{4l_{Body}}$) in proximity to earth's ground, which may result in reduced channel capacity and peak location around 37.5 MHz for a subject height of $\sim$2 m. In contrast, in the W2W setup, the increased Z_{retTx} and Z_{retRx} i.e., reduced C_{retTx} and C_{retRx}

respectively shift the body resonance peak to a higher frequency and enable the human body to act like a transmission line with broadband (i.e., low Q) resonance, resulting in increased channel capacity and peak location around 80 MHz or higher for a subject height of ∼2 m.

Supplementary Discussion 3: Subject's proximity to Metallic Object:

In the realm of human-machine interaction [3, 4], the practical deployment of this technology necessitates an examination of the robustness of the proposed wireless link. The underlying principle of operation relies on near-intermediate electric field-based coupling, making it sensitive to the presence of metallic objects in contact or proximity to the user's body. Such influences from metal structures can affect the received signal level and operational bandwidth, consequently impacting the channel's capacity for high-speed communication, as illustrated in the conceptual schematic shown in Fig. 2 (a). It can be inferred that when a BR HBC user comes into contact with a conducting or metallic object, a degradation in SNR and a reduction in bandwidth are to be expected due to an increase in effective channel length leading to higher loading, as depicted in Fig. 2 (b).

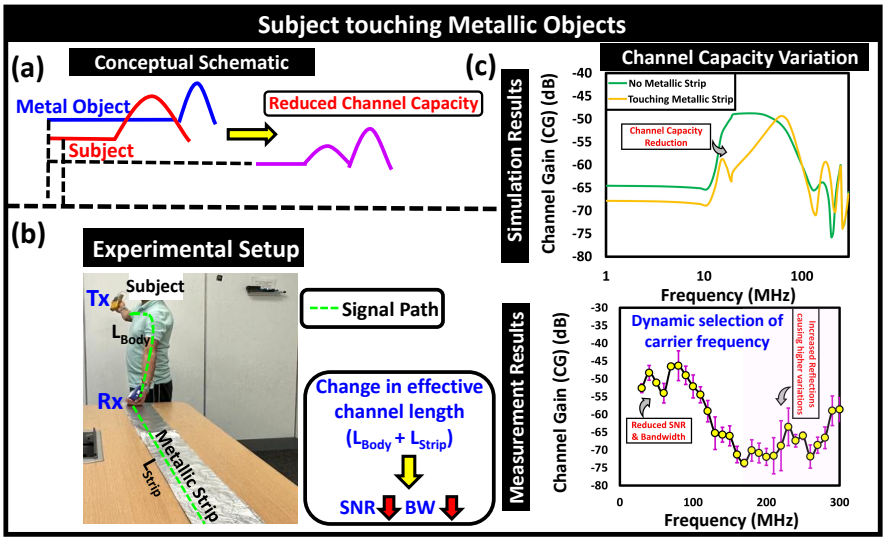

Fig. 2 Supplementary Figure 2: Influence of Conducting Objects presence in surroundings: a. Conceptual Schematic, **b.** Experimental Setup **c.** Simulation Results showing channel capacity reduction as a result of SNR degradation and attenuation in operational bandwidth from the increased effective length of the communication channel. **d.** Measured dataset showing increased variations in higher frequencies owing to the increase reflections from the metallic obejcts. The solution to these variabilities lies in dynamic selection of carrier frequency for optimum power allocation.

Furthermore, the results from numerical simulations and measurements presented in Fig. 2 (c) corroborate this understanding, revealing increased fluctuations in channel performance at higher frequencies resulting from enhanced reflections in the presence of additional conductive materials. These variabilities can be addressed through dynamic carrier frequency selection for optimal power allocation and adaptive matching at the devices. Now, from a circuit perspective, the proximity of conductive structures to the grounds of both the transmitting and receiving devices is expected to improve the received signal strength by lowering the impedance of their return paths (Z_{ret}), as illustrated by the relationship: $V_{Rx} \propto \frac{1}{Z_{ret-Tx} \cdot Z_{ret-Rx}}$. However, as the metallic object approaches the user's body, a significant shift occurs in the frequency boundary that distinguishes the non-radiative Electro-quasistatic (EQS) regime from the increased radiative nature of BR frequency regimes. This shift occurs at a lower frequency due to the increased body capacitance (C_{Body}), which modifies the relationship as follows: $f_{EQS-BR} \propto \frac{1}{C_{Body}}$.

Supplementary Discussion 4: BR HBC in Multi-Human Handshaking Channel:

In wireless communication, investigating the performance of a communication channel when it scales up to multiple users in a body-area network is crucial and hence portrayed in Fig. 3. The conceptual schematic of such a channel is presented in Fig. 3 (a), where a taller subject (height = 190 cm) with a transmitter operating in the BR regime shakes hands with a shorter subject (height = 168 cm) with a receiver, causes a partial overlapping of BR peaks of the individuals as illustrated in the experimental setup in Fig. 3 (b). The channel's measured performance is shown in Fig. 3 (c). From the field-theory perspective, for simplicity, assuming the body-channel length being L_{Body} for an individual, the increased no of users (N) in the network results in the increased channel length ($L_{net} = N \cdot L_{Body}$) that leads to low-frequency shift of the boundary between quasistatic near-field ($k \cdot r << 1$)-to-reactive electromagnetic intermediate field ($k \cdot r > 1$)-to- radiative far field ($k \cdot r >> 1$) limits as r increases with increased no. of users $r \propto N \cdot L_{Body}$. Now, from a circuit theory perspective, this scenario can also be viewed as resonators getting cascaded during such interaction and with more no. of network users, the more degradation of signal strength (V_{Rx}) is expected in comparison to a single user due to an increase in the effective body-ground coupling (i.e., Z_{BG}) as $V_{Rx} \propto Z_{BG} \propto \frac{1}{C_{Body}}$. Hence, with an attenuated SNR, the power efficiency may go down, but the throughput remains higher compared to its EQS and RF under identical scenarios.

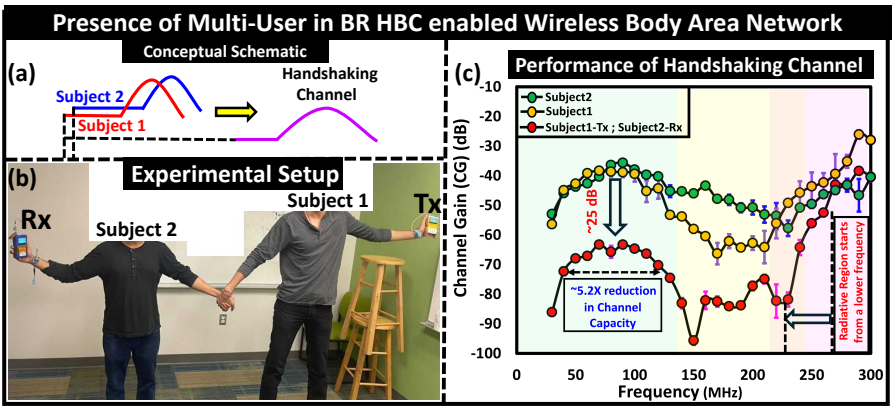

Fig. 3 Supplementary Figure 3: Presence of Multi-User in a BR HBC Network: **a.** Conceptual Schematic illustrating the overlap of the BR regime for the two subjects, **b.** Experimental Setup **c.** Performance of BR HBC in a handshaking channel.

Supplementary Discussion 5: BR HBC in context of the conventional wireless spectrum

There has been a significant trend towards the design of high-frequency wireless systems, particularly in the sub-THz and mm-wave ranges. However, these frequencies may not be ideal when considering the need for energy-efficient, high-speed connectivity among battery-powered wearable devices located around the body. They pose challenges such as high transmission path loss, a requirement for line-of-sight, and sensitivity to obstacles, etc. which can impede communication coverage and reliability. The constraints associated with enabling are body communication links at sub-THz and mm-wave bands are depicted below:

1. Higher Transmission Path Loss: mm-wave systems (frequencies between 30-300 GHz) with wavelengths ranging between 1-10 mm and sub-THz systems (frequencies between 300 GHz-3 THz) with wavelengths ranging between 100 µm-1 mm, owing to their orders of magnitude shorter wavelength compared to the human body dimension, incur higher signal attenuation (reduced signal strength) as it travels around the human body.

2. Scattering and Diffraction: High frequencies are also more susceptible to scattering and diffraction, making it difficult to maintain a stable connection in complex environments.

3. Requirement of Line-of-Sight (LOS) : With mm-wave in the higher part of the radio wave spectrum, sub-THz frequencies being even higher in the radio wave spectrum and extending into the terahertz region, these frequencies are more susceptible to blockage and require a clear line of sight between the transmitter and receiver for reliable communication. During the commonly encountered Non-Line-of-Sight scenario the higher loss incurred at these frequencies may not fit the bill with the supported link budget of battery-powered wearable devices.

4. Limited Coverage Area: The higher attenuation during propagation around the human body and LOS requirements for reliable operation results in significantly shorter communication coverage compared to the proposed BR HBC.
5. Higher Signal Leakage: With the operating frequency making transition to the mm-wave and sub-THz band, the increased far-field component of the transmitted signal increases the off-body signal which may pose security threats to the user's personal data.
6. Higher sensitivity around Body & Signal Degradation: The signal transmitted in the sub-THz, mm-wave frequency bands are highly susceptible to their change in transmission path i.e. they get more easily diffracted (bent) around the human body, leading to an increased interference between multiple propagation paths that can lead to signal degradation.
7. Technological Challenges: The limited availability of suitable components such as antennas, transceivers, and amplifiers etc. and need for modulation schemes making it more challenging to design and implement wireless systems for body area network devices at these frequencies.

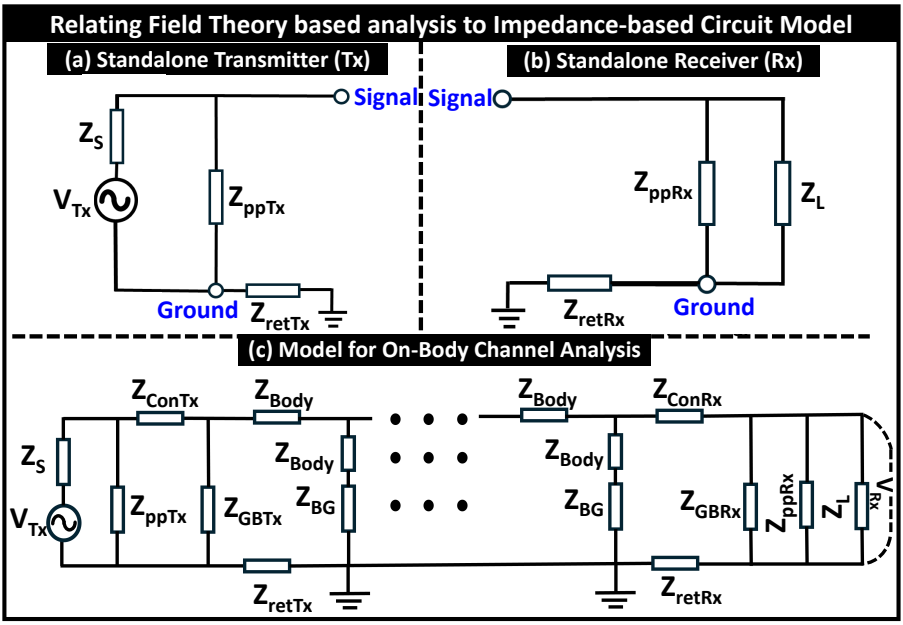

Fig. 4 Supplementary Figure 4: Conceptual Simplified Impedance-based Circuit Model: a. Model for standalone transmitter (Tx), **b.** Model for standalone receiver (Rx) **c.** Model for On-Body Channel Analysis

Supplementary Discussion 6: Relating Field-based understanding to Circuit Model

The fundamental-physics based study being the primary focus of this work, relating the field theory based understanding with the proposed conceptual model remains one of the central focus of this work. With single-ended excitation-pickup and voltage mode signaling, the impedance-based transfer function can be formulated as follows:
For an applied input excitation being V_{Tx}, assuming the voltage between the subject's body and Tx-ground being V_{in} at the location of transmitter, the device coupling efficiency ($\eta_{Tx-Body} = \frac{V_{Body}}{V_{Tx}}$) can be formulated as follows:

$$\frac{V_{in}(\omega)}{V_{Tx}(\omega)} = \frac{Z_{ppTx}}{Z_{ppTx} + Z_S} \cdot \frac{Z_{GBTx}}{Z_{GBTx} + Z_{ConTx}} \tag{1}$$

where Z_S is the source impedance of the transmitter, $Z_{ConTx}(\omega)$ denotes the contact impedance between the Tx-signal electrode and Body and Z_{ppTx} presents the signal plate-to-ground plate impedance and Z_{GBTx} stands for the parasitic impedance between Tx-ground and skin. Hence, $\eta_{Tx-Body}$ can be maximized by reducing Z_S, Z_{ConTx} and by increasing Z_{ppTx}, Z_{GBTx}.

Consequently, the potential distribution between the Tx and user's body can be written as

$$\frac{V_{Body}(\omega)}{V_{in}(\omega)} = \frac{Z_{BG} + Z_{Body}}{Z_{BG} + Z_{Body} + Z_{ret-Tx}} \tag{2}$$

where

$$Z_{Body}(\omega) = R_{Body}(\omega) + j \cdot X_{Body}(\omega)$$

and Z_{BG} is the parasitic impedance between the user's body to earth's ground. Now, with voltage mode pickup at the receiver, the output voltage can be represented as follows:

$$\begin{aligned} V_{Rx}(\omega) &= \frac{Z_{Leff}}{Z_{Leff} + Z_{ret-Rx} + Z_{ConRx}} V_{Body} \\ &= \frac{Z_{Leff}}{Z_{Leff} + Z_{ret-Rx} + Z_{ConRx}} \cdot \frac{Z_{BG} + Z_{Body}}{Z_{BG} + Z_{Body} + Z_{ret-Tx}} V_{in}(\omega) \end{aligned}$$

where $Z_{Leff} = Z_{ppRx} + Z_{GBRx}$ represents effective load impedance at the receiver comprising of the plate-to-plate impedance (Z_{ppRx}), impedance between Rx-ground-to-Body, and Z_{ConRx} denotes contact impedance between the user's body and Rx's signal electrode. At the receiving end the efficiency of voltage pickup ($\eta_{Body-Rx}$) can be expressed as:

$$\eta_{Body-Rx} = \frac{V_{Rx}(\omega)}{V_{Body}(\omega)} = \frac{Z_{Leff}}{Z_{Leff} + Z_{ret-Rx} + Z_{ConRx}} \tag{3}$$

Hence, $\eta_{Body-Rx}$ can be maximized by reducing Z_{ConRx}, Z_{ret-Rx} and increasing Z_{ppRx}, Z_{GBRx}. The on-body signal strength in relation to the input voltage can expressed as follows:

$$V_{Rx}(\omega) = \frac{Z_{Leff}}{Z_{Leff} + Z_{ret-Rx} + Z_{ConRx}} \cdot \frac{Z_{BG} + Z_{Body}}{Z_{BG} + Z_{Body} + Z_{ret-Tx}} \cdot \frac{Z_{ppTx}}{Z_{ppTx} + Z_S} \cdot \frac{Z_{GBTx}}{Z_{GBTx} + Z_{ConTx}} V_{Tx}(\omega) \tag{4}$$

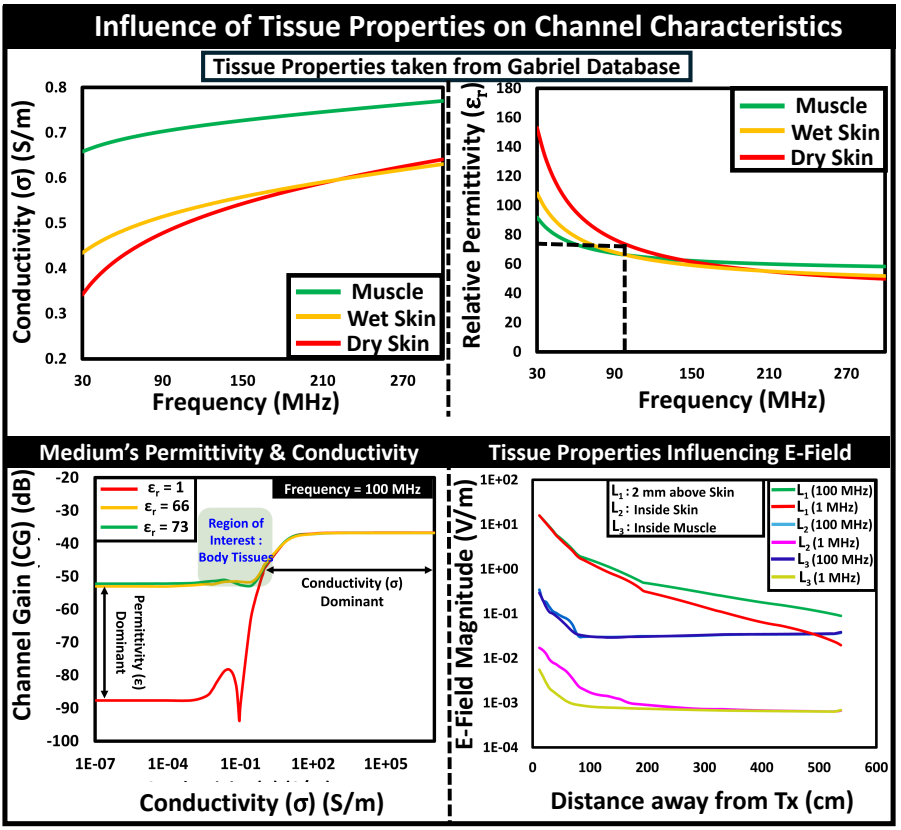

Fig. 5 Supplementary Figure 5: Influence of Tissue Properties on Channel Characteristics: a. Conductivity of body tissues, **b.** Relative Permittivity of body tissues adopted from the work of Gabriel et al. **c.** Conductivity sweep, **d.** Comparison of Electric Field magnitude in different tissue layers in EQS (1 MHz) and BR (100 MHz).

Supplementary Discussion 7: Influence of Tissue properties on Channel Characteristics

Considering the human body as a single-wire lossy transmission line may apparently introduce certain limitations: Specifically, the composition of the body may seem to affect the body resonance phenomenon, raising questions about how to account for performance variations across different individuals. To address this concern, we conducted numerical simulations to analyze the variability of the BR HBC channel in terms of changes in body composition, specifically by varying relative permittivity ($\epsilon_r(f)$) and bulk conductivity ($\sigma(f)$) on a simplified model made up of muscle as the inner core with a 4 mm skin layer as the outer covering. The frequency-dependent variation of $\epsilon_r(f)$ and $\sigma(f)$ of Body Tissues (i.e., muscle, dry skin, and wet skin) in the BR frequency Regime obtained from the Gabriel database [5] is plotted in Fig. 5 (a, b). In search of the underlying fundamentals, we artificially varied the ϵ_r and σ of body tissue. The variation in channel gain with change in conductivity for the relative permittivity of muscle, wet skin, and dry skin at different operating frequencies is presented in Fig. 5 (c). Moreover, we have also observed variation in the magnitude of electric field from the transmitter in three different scenarios: namely (a) 2 mm above skin, (b) Inside Skin, (c) Inside Muscle, we concluded that the E-Field magnitude remains higher above skin and decreases inside skin and goes on reducing even further inside muscle layer as it is more conductive than skin. In comparison, to EQS (operating frequency: 1 MHz), BR HBC (operating frequency: 100 MHz) experiences an increased magnitude of E-Field. From the results obtained, we conclude that the variability associated with the performance of the BR HBC channel remains within acceptable tolerance limits. With these variabilities within tolerance, the differences in channel gain across various subjects can be effectively managed by designing transceivers with user-specific adaptability. This means that when users of this technology wear a BR HBC transmitter, it establishes a personalized connection (based on body parameters derived from data obtained through body-connected sensors and actuators) with BR HBC receivers (the user's body-connected devices) during the handshaking processes.

Supplementary Discussion 8: Communication Specificity Comparison of BR HBC with Radiative Wireless

Traditional radio frequency (RF)-based communication uses antennas at the transceivers (i.e., transmitter and receiver) to transfer information via radiation. These antennas, depending upon their polarization patten, incurs substantial off-body leakage as their principle of operation relies on their broadcasting nature, hence causing security threats to users' personal information in the context of wireless body area networks. For quantification, let's assume a RF antenna in the transmitting mode radiates a signal with power P_{Tx} and

with antenna gain being G_{Tx}. The radiated power density at a distance r from the antenna can be approximated as:

$$P_D = P_{Tx} \cdot G_{Tx}/4\pi r^2 \tag{5}$$

Owing to its conductivity and water content, the human body absorbs, reflects and scatters some fraction of the radiated signal, and the amount of signal loss depends on the tissue properties and the frequency. Now, for another antenna operating in the receiving mode, the Friis transmission equation, forms the basis for estimating its received power (P_{Rx1}) in free space which takes the following form:

$$P_{Rx1} = P_{Tx} \cdot G_{Tx} \cdot G_{Rx} \cdot \frac{\lambda}{4\pi r^2} \tag{6}$$

Where, G_{Rx} = Gain of the receiving antenna, λ = Wavelength (c/f, where c is the speed of light and f is the operating frequency), r = Distance between antennas. For simplification, assuming line-of-sight scenario, the above expression P_{Rx1} gets modified in the presence of the human body to take the body's influence into account (i.e., loss factor α and path-loss exponent n) and becomes:

$$\begin{aligned} P_{Rx1} &= P_{Tx}G_{Tx}G_{Rx}(\lambda/4\pi)^2/(r^2 \cdot (1 + \alpha_1 r^{n_1})) \\ &= P_{Tx}G_{Tx}G_{Rx}(\lambda/4\pi)^2/[r^2 + \alpha_1 r^{2+n_1}] \end{aligned} \tag{7}$$

Assuming, a third antenna operating in receiving mode is located in the operational field of the RF-transmitter but away from the human body intended to pick up the off-body leakage, with ideal, lossless transmission path in a line-of-sight scenario, the received power can be written as:

$$\begin{aligned} P_{Rx2} &= P_{Tx}G_{Tx}G_{Rx}(\lambda/4\pi)^2/(r^2 \cdot (1 + \alpha_2 r^{n_2})) \\ &= P_{Tx}G_{Tx}G_{Rx}(\lambda/4\pi)^2/[r^2 + \alpha_2 r^{2+n_2}] \end{aligned} \tag{8}$$

Hence,

$$\frac{P_{Rx1}}{P_{Rx2}} = \frac{V_{Rx1}^2}{V_{Rx2}^2} = \frac{r^2 + \alpha_2 r^{2+n_2}}{r^2 + \alpha_1 r^{2+n_1}} = \frac{(1 + \alpha_2 r^{n_2})}{(1 + \alpha_1 r^{n_1})} \tag{9}$$

where, $\frac{V_{Rx1}}{V_{Rx2}}$ represents the communication specificity (CS) as the ratio of on-body to off-body signal strength assuming iso sensitivity and iso-termination for the two receivers for a certain transmit power. In the context of wearables (size $\leq$ 3 cm) i.e., electrically short antennas, with Bluetooth operating within the 2.4 to 2.485 GHz frequency band, which corresponds to a wavelength (λ) of $\sim$6 cm to 12.5 cm, making the field of observation (r $\geq$ 1 m) to be in the far field region ($r > 2\lambda$). With the Rx1 experiencing more attenuation from the body, i.e., $\alpha_1 >> \alpha_2$ and $n_1 > n_2$ the specificity factor reduces with comparable or higher off-body signal strength.

Now, for an iso-form factor, iso-sensitivity off-body voltage mode receiver, the received signal strength can be obtained as follows: since from the numerical simulations and measurements we observed that the Tx side experiences

more leakage, hence we started our analysis with the leakage from a standalone BR HBC transmitter. the leakage signal strength from a standalone Tx can be expressed as:

$$V_{Leakage-Tx} = \frac{Z_{ppTx}}{Z_{ppTx} + Z_S} \cdot \frac{Z_{LeffRx2}}{Z_{LeffRx2} + Z_{Tx-Rx2} + Z_{ret-Rx2} + Z_{ret-Tx}} V_{in} \tag{10}$$

where $Z_{LeffRx2}$ and $Z_{ret-Rx2}$ respectively represent the effective load impedance and the return path impedance of the off-body receiver, and Z_{Tx-Rx2} denotes the impedance between Tx and Rx2. Now, when the Rx2 is present closer to the human body in comparison to Tx, the leakage contribution from the human body can be expressed as:

$$V_{Leakage}(\omega) = \frac{Z_{ppTx}}{Z_{ppTx} + Z_S} \cdot \frac{Z_{GBTx}}{Z_{GBTx} + Z_{ConTx}} \frac{Z_{Body} + Z_{BG}}{Z_{Body} + Z_{BG} + Z_{ret-Tx}} \cdot \frac{Z_{LeffRx2}}{Z_{LeffRx2} + Z_{Body-Rx2} + Z_{ret-Rx2}} \cdot V_{Tx}(\omega) \tag{11}$$

where, $Z_{Body-Rx2}$ denotes the impedance of the signal path between body and the off-body receiver. Hence for BR HBC, CS is defined as $V_{Rx}/V_{Leakage}$.

References

[1] Datta, A., Nath, M., Yang, D., Sen, S.: Advanced biophysical model to capture channel variability for eqs capacitive hbc. IEEE Transactions on Biomedical Engineering (2021)

[2] Modak, N., Das, D., Nath, M., Chatterjee, B., Kumar, G., Maity, S., Sen, S.: Eqs res-hbc: A 65-nm electro-quasistatic resonant 5–240 μw human whole-body powering and 2.19 μw communication soc with automatic maximum resonant power tracking. IEEE Journal of Solid-State Circuits **57**(3), 831–844 (2022)

[3] Maity, S., Yang, D., Redford, S.S., Das, D., Chatterjee, B., Sen, S.: Bodywire-hci: Enabling new interaction modalities by communicating strictly during touch using electro-quasistatic human body communication. ACM Transactions on Computer-Human Interaction (TOCHI) **27**(6), 1–25 (2020)

[4] Sarkar, S., Yang, D., Nath, M., Datta, A., Maity, S., Sen, S.: Human-structure and human-structure-human interaction in electro-quasistatic regime. Communications Engineering **4**(1), 26 (2025)

[5] Gabriel et al., S.: The dielectric properties of biological tissues: II. measurements in the frequency range 10 hz to 20 GHz. Physics in Medicine and

Biology **41**(11), 2251–2269 (1996). https://doi.org/10.1088/0031-9155/41/11/002

Additional information:

Additional supplementary information is available at https://github.com/SparcLab/BodyResonanceHBC. Correspondence and requests for materials should be addressed to Shreyas Sen (shreyas@purdue.edu) or Samyadip Sarkar.